

# Pressure-Induced Zero-Gap Semiconducting State in Organic Conductor $-(\text{BEDT-TTF})_2\text{I}_3$ Salt

Shinya Katayama, Akiyo Kobayashi and Yoshikazu Suzumura

Department of Physics, Nagoya University, Nagoya 464-8602

(Received December 5, 2005)

We show a zero-gap semiconducting (ZGS) state in the quasi-two-dimensional organic conductor  $-(\text{BEDT-TTF})_2\text{I}_3$  salt, which emerges under uniaxial pressure along the *a*-axis (the stacking axis of the BEDT-TTF molecule). The ZGS state is the state in which a Dirac cone with the band spectrum of a linear dispersion exists around the Fermi point connecting an unoccupied (electron) band with an occupied (hole) band. The spectrum exhibits a large anisotropy in velocity, which depends on the direction from the Fermi point. By varying the magnitude of several transfer energies of a tight-binding model with four sites per unit cell, it is shown that the ZGS state exists in a wide pressure range, and is attributable to the large anisotropy of the transfer energies along the stacking axis.

**KEYWORDS:** organic conductor, BEDT-TTF, quarter-filling, tight-binding model, zero-gap semiconductor, Dirac cone, contact point,  $-(\text{BEDT-TTF})_2\text{I}_3$ ,

## 1. Introduction

Quasi-two-dimensional organic conductors, BEDT-TTF (bis(ethylene-dithio)tetrathiafulvalene) salts, exhibit several electronic states, such as Mott insulator, charge ordering and superconductivity,<sup>1,2</sup> under the variation of temperature, hydrostatic pressure or uniaxial strain. The electronic states of these BEDT-TTF (ET) salts originate from  $\pi$ -electrons with the several transfer energies and the strong Coulomb interaction acting on-site and between nearest-neighbor sites. Among these salts, unusual phenomena have been observed in the  $-(\text{ET})_2\text{I}_3$  (phase of BEDT-TTF tri-iodide) salt,<sup>3</sup> which consists of four molecules per unit cell with a 3/4-filled band (i.e., quarter-filled band of the hole). Under ambient pressure (AP), the  $-(\text{ET})_2\text{I}_3$  salt exhibits the metal-insulator transition at  $T_{\text{MI}} = 135$  K, which is followed by charge ordering<sup>4,9</sup> along the *b*-direction perpendicular to the stacking axis (*a*-axis). When a uniaxial strain at 2 kbar is applied along the *a*-direction, the salt undergoes the superconducting transition at 7 K.<sup>10,11</sup> Under high pressures, the  $-(\text{ET})_2\text{I}_3$  salt shows exotic properties, that are consistent with the narrow gap semiconducting (NGS) state.<sup>5,6</sup> At 20 kbar of the hydrostatic pressure, resistivity becomes metallic and is almost independent of temperature between 300 K and 1.5 K, although carrier density,  $n$ , decreases from  $10^{21}$  cm<sup>-3</sup> (300 K) to  $10^{15}$  cm<sup>-3</sup> (1 K). It has been claimed that such a temperature dependence may originate from the NGS state with a gap  $E_g \sim 1$  meV.<sup>6</sup> There exists a difference in the effect of uniaxial pressure between the *a*-direction ( $P_a$ ) and the *b*-direction ( $P_b$ ).<sup>11</sup> For a compression along the *a*-direction, the pressure dependence of  $T_{\text{MI}}$  is small and the NGS state is likely to be realized for  $P_a > 5$  kbar. For the uniaxial strain along the *b*-direction, the metal-insulator transition is suppressed noticeably, whereas neither superconducting transition nor NGS state occurs at low temperatures.

The ordered state in  $-(\text{ET})_2\text{I}_3$  has been investigated theoretically; a charge ordering state with the horizontal

pattern was obtained using the Hartree-Fock approximation<sup>12,15</sup> and the superconducting state in the presence of the charge ordering was clarified in terms of the random phase approximation.<sup>16,17</sup> It is noted that such a superconducting state occurs just before the onset of the NGS state under the *a*-axis pressure. However, the origin of the NGS state is not yet clear, although only the uniaxial pressure along the *a*-axis leads to the NGS state in the  $-(\text{ET})_2\text{I}_3$  salt.

In the present paper, we examine the pressure dependence of the band structure of the  $-(\text{ET})_2\text{I}_3$  salt within the tight-binding model in order to understand the NGS state, which emerges and remains in a wide range of the uniaxial pressure along the *a*-axis. In x2, we study the pressure dependence by assuming an extrapolation formula for the pressure dependence of transfer energies of the  $-(\text{ET})_2\text{I}_3$  salt. We employ the data obtained from the X-ray diffraction experiment under pressures along both the *a*-axis and the *b*-axis.<sup>18,20</sup> In x3, it is shown that the present organic conductor under high pressures exhibits a zero-gap semiconducting (ZGS) state with a Dirac-cone-like linear dispersion instead of the NGS state. The origin of the ZGS state under pressure is analyzed by varying parameters of transfer energy in x4. We also investigate the ZGS state in x5 by using a reduced model with two sites in the unit cell. Section 6 is devoted to the summary and discussion.

## 2. Formulation

In order to describe conduction electrons for the  $-(\text{ET})_2\text{I}_3$  salt, we start with a two dimensional lattice model, which consists of four ET molecules in the unit cell as shown in Fig. 1. The Hamiltonian is given by

$$H = \sum_{n,m} \sum_{i,j} t_{i,j} c_{i,n}^\dagger c_{j,m} ; \quad (1)$$

where  $t_{i,j}$  is the transfer energy from the ( $j$ ; ) site to the nearest-neighbor (*n.n.*) ( $i$ ; ) site. In eq. (1),  $i$  and  $j$  ( $= 1; 2, 3, 4$ ) denote the unit cells of the square lat-

tice. The indices and denote the four molecules in the unit cell, where 1, 2, 3 and 4 correspond to A, A', B and C in ref. 18, respectively.  $c_i$  is the annihilation operator of the conduction electron at the ( $i$ ; ) site. Using

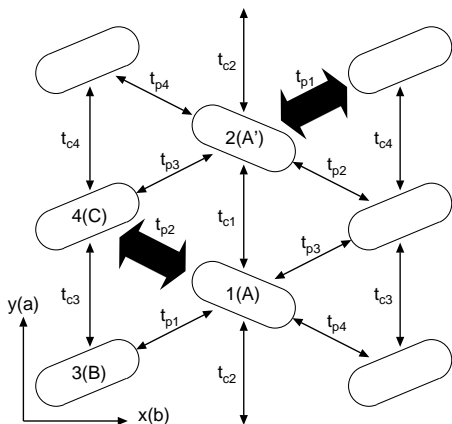


Fig. 1. Conducting plane of  $-(\text{ET})_2\text{I}_3$ , where there are four ET molecules in the unit cell and the bond represents eight transfer energies ( $t_{p1}$ ;  $t_{p2}$ ;  $t_{p3}$ ;  $t_{p4}$ ;  $t_{c1}$ ;  $t_{c2}$ ;  $t_{c3}$ ;  $t_{c4}$ ). The  $x$  ( $y$ )-axis corresponds to the  $b$  ( $a$ )-axis in ref. 18. Thick arrows denote the dimerization in a model, which is considered in x5.

the Fourier transformation,  $c_i = N_L^{-1/2} \sum_k e^{ik \cdot r_i} c_k$ , eq. (1) is rewritten as

$$H = \sum_{k; j} \sum_{k'} (k)_{j k'} c_k^\dagger c_{k'} \quad (2)$$

where

$$(k)_{ij} = \frac{1}{N_L} \sum_{i'j'} t_{i'j'} e^{ik \cdot (r_{i'} - r_{j'})} \quad (3)$$

and  $t_{i'j'}$  represents eight transfer energies given by  $t_{p1}$ ;  $t_{p2}$ ;  $t_{p3}$ ;  $t_{p4}$ ;  $t_{c1}$ ;  $t_{c2}$ ;  $t_{c3}$ ;  $t_{c4}$ ; as shown in Fig. 1. In eq. (2),  $(k)$  is expressed as

$$\begin{aligned} (k)_{11} &= 0 \quad (i = 1; j = 1); \\ (k)_{12} &= t_{c1} + t_{c2} e^{ik_y}; \\ (k)_{13} &= t_{p1} - t_{p4} e^{ik_x}; \\ (k)_{14} &= t_{p2} - t_{p3} e^{ik_x}; \\ (k)_{23} &= t_{p4} e^{ik_y} - t_{p1} e^{i(k_x + k_y)}; \\ (k)_{24} &= t_{p3} - t_{p2} e^{ik_x}; \\ (k)_{34} &= t_{c3} + t_{c4} e^{ik_y}; \end{aligned} \quad (4)$$

where  $k_x$  is replaced by  $k_x + \pi$ , and the summation  $\sum_{k'} (y)$  corresponds to the  $b$  ( $a$ )-axis.<sup>18</sup> The chemical potential determined by the 3/4 filling is set to zero in order to take the Fermi energy as the origin of the band spectrum.

For the pressure dependence of transfer energies  $t_{i'j'} = t_A^0 (A = c1; c4; p1; p4)$  of  $-(\text{ET})_2\text{I}_3$ , we employ an extrapolation formula given by<sup>16</sup>

$$t_A(P_a) = t_A^0 (1 + K_A P_a); \quad (5)$$

$$t_A^0(P_b) = t_A^0 (1 + K_A^0 P_b); \quad (6)$$

where  $t_A(P_a)$  ( $t_A^0(P_b)$ ) represents the transfer energy under the pressure  $P_a$  ( $P_b$ ) along the  $a$ -axis ( $b$ -axis). Hereafter, the units of pressure and transfer energy are taken as kbar and eV, respectively. By using the data of  $-(\text{ET})_2\text{I}_3$  salt for ambient pressure ( $P_a = P_b = 0$ )<sup>18</sup> and those for  $P_a = 2$  and  $P_b = 3$  at room temperature,<sup>19,20</sup> the above coefficients are estimated as  $t_{p1} = 0.140$ ,  $t_{p2} = 0.123$ ,  $t_{p3} = 0.025$ ,  $t_{p4} = 0.062$ ,  $t_{c1} = 0.048$ ,  $t_{c2} = 0.020$ ,  $t_{c3} = 0.028$ ,  $t_{c4} = 0.028$  at ambient pressure and  $K_{p1} = 0.011$ ,  $K_{p2} = 0.0$ ,  $K_{p3} = 0.0$ ,  $K_{p4} = 0.032$ ,  $K_{c1} = 0.167$ ,  $K_{c2} = 0.025$ ,  $K_{c3} = 0.089$  and  $K_{c4} = 0.089$  ( $K_{p1}^0 = 0.024$ ,  $K_{p2}^0 = 0.031$ ,  $K_{p3}^0 = 0.053$ ,  $K_{p4}^0 = 0.022$ ,  $K_{c1}^0 = 0.042$ ,  $K_{c2}^0 = 0.133$ ,  $K_{c3}^0 = 0.167$  and  $K_{c4}^0 = 0.167$ ) for pressures along the  $a$ -axis ( $b$ -axis). As seen from  $K_A$ , the large  $K_{c1}$  suggests that the pressure dependence along the  $a$ -axis is mainly determined by  $t_{c1}$ .

### 3. ZGS State

In this section, we focus on the electronic states under the pressure along the  $a$ -axis, i.e.,  $P_a$ . Since there are four sites in the unit cell, there are four energy bands which are obtained by diagonalizing eq. (2). The first band with the highest energy is almost empty and the second one is almost filled due to 3/4-filling. Whereas there is a small electron pocket close to the  $X(0; \pi)$  point and a hole pocket close to the  $Y(0; 0)$  point at ambient pressure,<sup>6</sup> these pockets are reduced at  $P_a = 2$ <sup>19,20</sup> and they are further reduced to a point in a wide range of higher pressures.<sup>16,17</sup> Actually from eq. (5), it is found that such an unusual state is stable for  $P_a > 3$ .

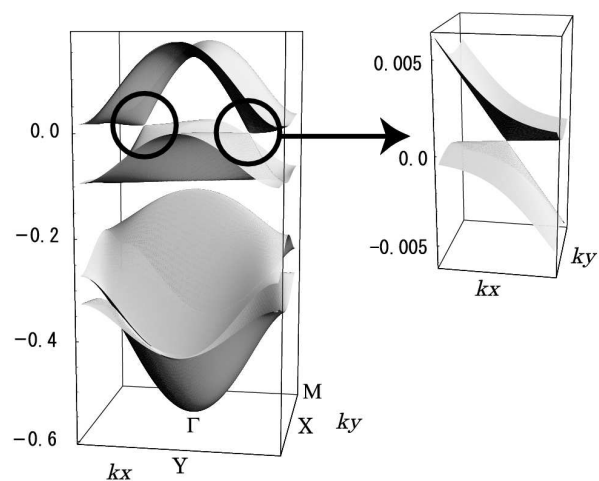


Fig. 2. Band dispersion of  $-(\text{ET})_2\text{I}_3$  at  $P_a = 4$  kbar in the Brillouin zone (left panel) and enlarged one around contact point at  $k^0 = (0.602; 0.353)$  (right panel), where Fermi energy is taken as origin.

Figure 2 shows the energy band spectrum of  $-(\text{ET})_2\text{I}_3$  at  $P_a = 4$  (left panel) in the plane of  $k_x$  and  $k_y$ , which is scaled by the inverse of the lattice constant. The first band is unoccupied, whereas the second band is occupied. It should be noted that the first and second bands touch at the points  $k^0$  as shown with the circle. This

contact point becomes the Fermi point due to 3/4-lling. Actually, the matrix elements of eq. (4), corresponding to  $k^0 = (0.602; 0.353)$ , are  $\mu_{12} = 0.072 - 0.016i$ ;  $\mu_{13} = 0.124 + 0.066i$ ;  $\mu_{14} = 0.115 + 0.024i$ ;  $\mu_{23} = 0.135 - 0.040i$ ;  $\mu_{24} = 0.014 - 0.117i$  and  $\mu_{34} = 0.055 - 0.034i$ . The four band energies are given as 0, 0, -0.210, -0.477, in which the Fermi energy is given by  $\epsilon_F = 0.172$ . The existence of such a point implies that the hole and electron bands are degenerate at the point. Since the point has no relation to the symmetry, such a degeneracy occurs accidentally as first pointed out by Herring.<sup>21</sup>

It should be noted in the enlarged figure (right panel of Fig. 2) that a linear dispersion is present around the contact point  $k^0$ . Such a state always exists for  $P_a > 3$ . The dispersion close to the point can be expressed as

$$E^{\pm}(k) = v^{\pm}(k)k - k^0_j; \quad (7)$$

where  $k = k - k^0$ , and  $v^+(k)$  ( $v^-(k)$ ) is the velocity for the electron (hole). We call such a state the Dirac cone, according to the literature.<sup>22(25)</sup> In Fig. 3, the velocity  $v^{\pm}(k)$  is shown as a function of  $\theta$ , which is the angle between the vector  $k$  and the  $k_x$ -axis. A noticeable angular variation in velocity is seen with the relation:

$$v^+(k) \notin v^-(k); \quad (8)$$

$$v^+(k) = v^-(k); \quad (9)$$

within the numerical accuracy of the present calculation.

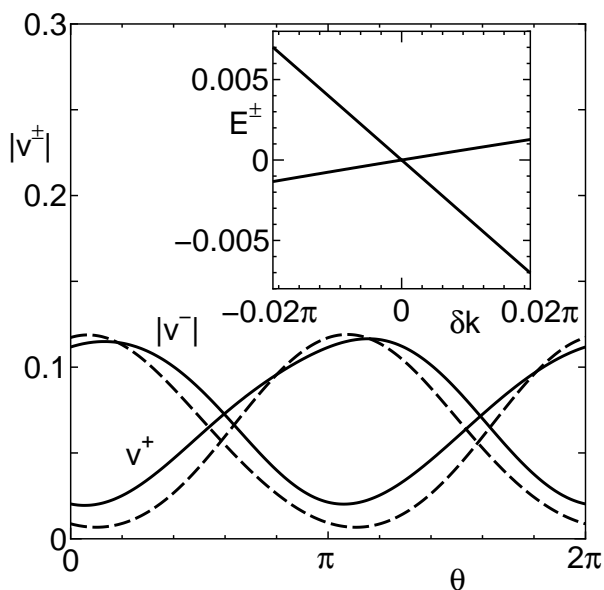


Fig. 3. Angular dependence of velocity around contact point, i.e., Dirac cone at  $P_a = 10$  (solid line) and 5 (dashed line), where horizontal axis denotes angle  $k = k - k^0$  and the  $k_x$ -axis. The inset shows  $E^{\pm}(k)$  at  $P_a = 10$ , where  $k > 0$  and  $< 0$  correspond to  $\theta = 0$  and  $\pi$ , respectively.

For both low and high pressures, the schematic band dispersion is shown in Fig. 4, where the crossing in the band spectrum denotes the contact point which is located at the bottom of the electron band. At low pressures

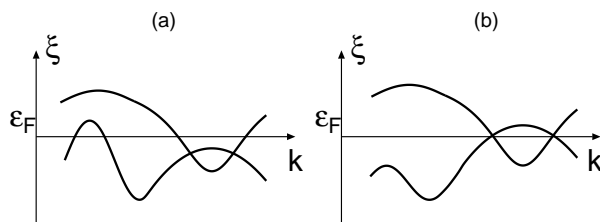


Fig. 4. Schematic band dispersion of metallic state at low pressure (a) and that of ZGS state at high pressure (b), where wave number  $k$  (horizontal axis) is chosen so as to include contact point.

(Fig. 4 (a)) with  $P_a \lesssim 3$ , one finds a metallic state where two contact points at  $k^0$  and  $-k^0$  exist below the Fermi energy  $\epsilon_F$ . However, at high pressures (Fig. 4 (b)) with  $P_a \gtrsim 3$ , the contact point is located just at the Fermi energy, i.e., the realization of the ZGS, which is retained due to the 3/4-lling for a wide pressure range. The ZGS state shows up in the density of states  $D(\epsilon)$  close to the Fermi energy as<sup>16</sup>

$$D(\epsilon) \propto |\epsilon - \epsilon_F|; \quad (10)$$

where  $\epsilon = \epsilon_F$  corresponds to the Fermi energy. Since  $D(\epsilon)$  vanishes at  $\epsilon = \epsilon_F$ , we call the state with eq. (10) the ZGS state instead of the NGS state.<sup>6,16</sup> Although the contact point still remains in the metallic state at low pressure, the corresponding cusp in the density of states is reduced and becomes invisible for  $P_a \gtrsim 2.5$ .

In Fig. 5, the pressure dependence of the point contact,  $k^0$ , is examined, where the Fermi surface is shown for ambient pressure and  $P_a = 2$ . With increasing pressure, the area of the Fermi surface is reduced as seen from the electron (hole) pocket around the X (Y) point.<sup>19</sup> The symbols on the arrow  $P_a$  represent the location of contact points at  $P_a = 0, 2$  and 3, respectively. The arrow  $P_a$ , which denotes the trajectory of  $k^0$  from  $P_a = 0$  to  $P_a = 10$ , extends to the direction of the point with increasing  $P_a$ . The contact point is located below the Fermi surface for  $P_a < 3$  and just on the Fermi surface for  $3 < P_a < 10$ . The arrow  $P_b$ , which corresponds to that of  $k^0$  for  $0 < P_b < 10$ , is discussed in x6.

#### 4. Stability of Contact Point

In order to examine the stability of the contact point against the change in parameters, we calculate the energy band spectra by varying magnitudes of the transfer energies from those of  $-(E_T)_2 I_3$ . Since the difference between  $t_{c1}$  and  $t_{c2}$  is large for  $-(E_T)_2 I_3$ , we employ a model, in which  $t_{c1} \neq t_{c2}$  and the remaining parameters are chosen as

$$t_{p1} = t_{p2} = 1; t_{p3} = t_{p4}; \quad (11)$$

Thus, we examine a simplified model with independent parameters,  $t_{c1}, t_{c2}, t_{p3}$  and  $t_{c3}$ .

Figure 6 shows phase diagram in the plane of  $t_{c1}$  and  $t_{c2}$  for fixed  $t_{p3} (= t_{p4} = t_{c3} = t_{c4}) = 0.25$ . The contact points exist in regions I and II, which correspond to Figs. 4 (b) and 4 (a), respectively. Region I exhibits the ZGS state, where the point becomes equal to the Fermi

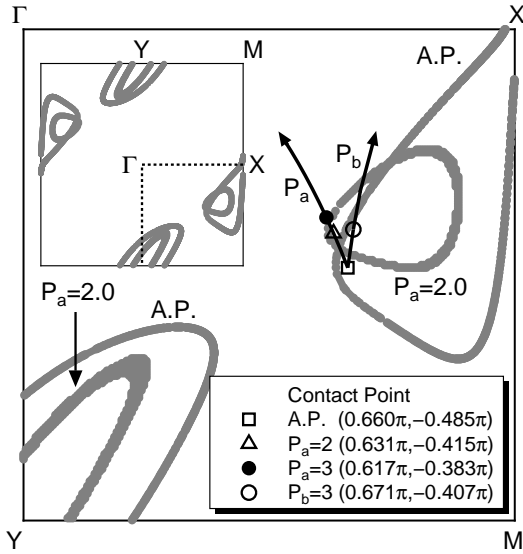


Fig. 5. Fermi surface (FS) of  $-(ET)_2I_3$  at ambient pressure and  $P_a = 2$ , where main (inset) figure corresponds to quarter (full) part of Brillouin zone. The arrow  $P_a$  denotes the pressure dependence of the contact point  $k^0$  for  $0 < P_a < 10$ , whereas the arrow  $P_b$  corresponds to  $k^0$  for  $0 < P_b < 10$ . The square, triangle, and filled circle represent  $k^0$  for  $P_a = 0, 2$ , and  $3$  respectively, while the open circle denotes that for  $P_b = 3$ .

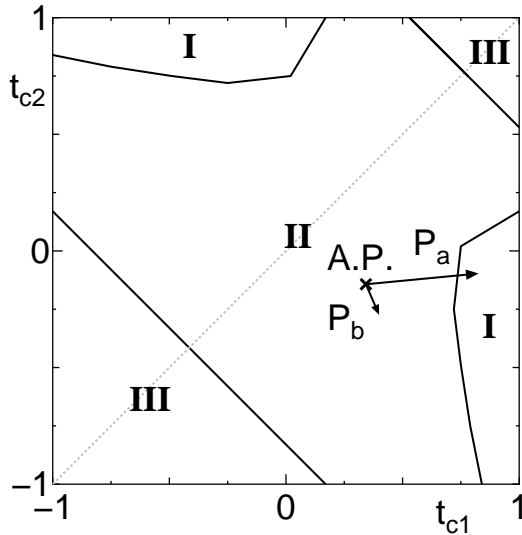


Fig. 6. Phase diagram on plane of  $t_{c1}$  and  $t_{c2}$  for  $t_{p3} = t_{p4} = t_{c3} = t_{c4} = 0.25$ , where transfer energies  $t_{c1}$  and  $t_{c2}$  are also normalized by  $t_{p1}$  ( $= t_{p2}$ ). The arrow denotes the variation in  $(t_{c1}; t_{c2})$  estimated from eq. (5) for  $0 < P_a < 10$  and  $0 < P_b < 5$ , respectively, where the cross corresponds to ambient pressure.

point. Region II corresponds to the metallic state with the point located below the Fermi energy. In Region III, the contact point disappears and the conventional metallic state is found. The boundary between regions II and III is given by

$$t_{c1} + t_{c2} = r_1; \quad t_{c1} - t_{c2} = r_2; \quad (12)$$

where  $r_1 = 1.53$  and  $r_2 = 0.83$ . Such a straight line of the boundary is due to the choice of the parameter  $t_{p3} = t_{p4} = t_{c3} = t_{c4}$ . When parameters  $t_{c1}$  and  $t_{c2}$  take

the value on the boundary of  $r_1$  ( $r_2$ ), the contact point is given by the (X) point on the  $k_x$ - $k_y$  plane in Fig. 5. Region I corresponds to a large  $t_{c1}$  and a negative  $t_{c2}$  (or a large  $t_{c2}$  and a negative  $t_{c1}$ ). Note that the case of  $t_{c1} = t_{c2}$  (dotted line in Fig. 6) gives the metallic state with a special situation where the first band has the same energy as the second band on the line  $k_y =$  in the Brillouin zone. The contact point disappears on this line. The van Hove singularity in the density of states exists near the Fermi energy when the parameters in region I move close to region II. When  $t_{p3j}$  ( $= t_{p4j}$ ) and  $t_{c3j}$  ( $= t_{c4j}$ ) are decreased, the area of region II is reduced.

Here, we comment on the pressure dependence of the contact point in Fig. 6. Here the arrow denotes the variation of  $t_{c1}$  and  $t_{c2}$  under the uniaxial pressures,  $P_a$  and  $P_b$ . From the comparison of these two arrows, it is found that the increase in  $P_a$  leads to the ZGS state but that in  $P_b$  is away from the ZGS state since the increase in  $t_{c1}$  is large enough for  $P_a$  but is small for  $P_b$ .

## 5. Reduced Model for ZGS State

The condition for the ZGS state with contact points depends on the transfer energies, although some of them are redundant. In  $x3$ , the ZGS state was obtained for the model shown in Fig. 1. It consists of four sites in the unit cell. However, the model is complicated to examine the ZGS state analytically. In order to understand clearly the ZGS state, we reduce further the number of parameters to obtain a model with two sites per unit cell.<sup>26</sup> There are other reduced models reproducing the energy band spectrum of  $(ET)_2X$ ,<sup>13,15</sup> which will be discussed in the next section.

First, we ignore four transfer energies,  $t_{p3}$ ;  $t_{p4}$ ;  $t_{c3}$  and  $t_{c4}$ , in Fig. 1, since the ZGS state with contact points exists even for  $t_{p3} = t_{p4} = t_{c3} = t_{c4} = 0$ . However, such a choice is not realistic for  $-(ET)_2I_3$  at  $P_a = 0$  due to the absence of the metallic state as shown later. Next, for the simplicity of the calculation, we reduce the number of molecules by considering the dimerization for the bond  $t_{p2}$  between 1 and 4 sites (and also that for  $t_{p1}$  between 2 and 4 sites), which is shown by the thick arrow in Fig. 1. With such a procedure, Fig. 1 can be replaced by Fig. 7, where we obtain an anisotropic square lattice consisting of two sites per unit cell. Thus, the reduced model is described by the Hamiltonian

$$H = \begin{pmatrix} 0 & T \\ T & 0 \end{pmatrix};$$

$$T = t_{p1} + t_{p2}e^{ik_y} \quad t_{c1}e^{i(k_x + k_y)} \quad t_{c2}e^{ik_x}; \quad (13)$$

with a half-filled band. Hereafter, we set  $t_{p1} = t_{p2} (= 1)$  for simplicity. Two bands are degenerate at  $k^0$  when the off-diagonal component of eq. (13) vanishes. The wave vector, at which the degeneracy occurs, can be obtained analytically as

$$k_x^0 = 2 \tan^{-1} \frac{r \frac{t_{c1} - t_{c2}}{2 + t_{c1} + t_{c2}}}{2 + t_{c1} + t_{c2}}; \quad k_y^0 = 2 \tan^{-1} \frac{p \frac{(2 - t_{c1} - t_{c2})(2 + t_{c1} + t_{c2})}{t_{c2} - t_{c1}}}{t_{c2} - t_{c1}}; \quad (14)$$

Equation (13) gives a symmetric linear dispersion of the Dirac cone with  $v^+(k) = v^-(k)$ . It is slightly different from eq. (7).

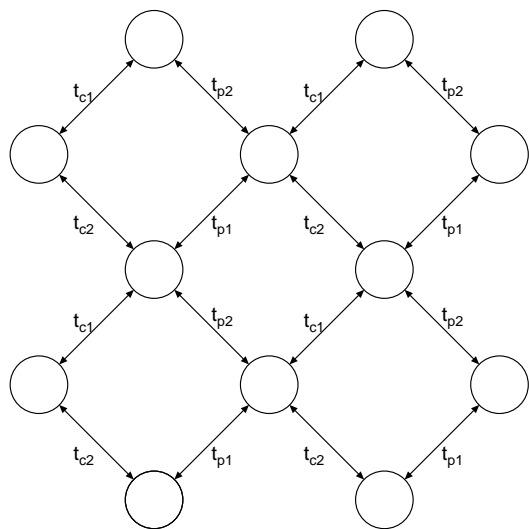


Fig. 7. Reduced model with anisotropic square lattice, which is obtained from Fig. 1. Here two sites are present in unit cell.

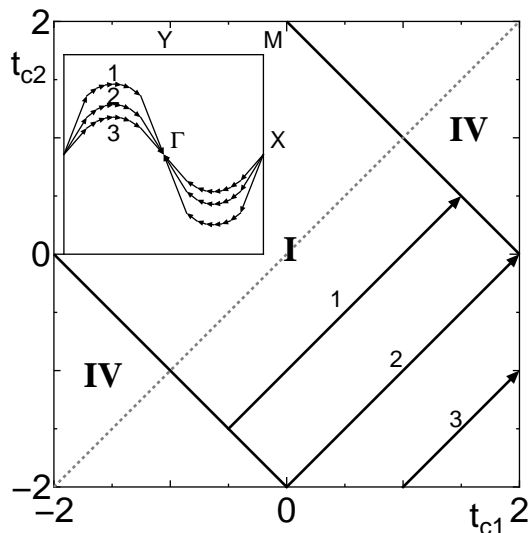


Fig. 8. Phase diagram on  $t_{c1}$ - $t_{c2}$  plane for the reduced model given by Fig. 7. Region I is the same as that in Fig. 6, whereas region IV corresponds to the insulating state. The dotted line shows  $t_{c1} = t_{c2}$ , where the upper and lower bands are degenerate on the zone boundary. The inset shows the trajectory of two contact points, when  $t_{c1}$  and  $t_{c2}$  are varied as the arrow in the main frame.

Figure 8 shows the  $t_{c1}$ - $t_{c2}$  phase diagram obtained from the model of Fig. 7. The ZGS state is realized in region I and the insulating state is obtained in region IV, respectively. The inset shows the locations of contact points in the  $k_x$ - $k_y$  plane, which are obtained from eq. (14) when parameters  $t_{c1}$ - $t_{c2}$  are varied as

$$(C_t = 1; 2; 3)$$

$$t_{c2} = t_{c1} + C_t ; \quad (15)$$

The corresponding parameters are shown by the arrow with 1, 2 and 3 in the main frame. The boundary between I and IV is given by

$$t_{c2} = t_{c1} - 2 ; \quad (16)$$

respectively. The properties of the contact point are as follows. The contact point is located at X for  $t_{c2} = t_{c1} - 2$ , and at  $\Gamma$  for  $t_{c2} = t_{c1} + 2$ , whereas the contact point is present near the zone boundary of the  $k_x$ - $k_y$  plane for  $t_{c1} < t_{c2}$ . When  $t_{c1} = t_{c2}$  holds, two bands are degenerate on the zone boundary and the contact point disappears. These facts indicate that the contact point comes from the symmetry breaking of the bond due to  $t_{c1} \neq t_{c2}$ .

From Fig. 8, it is found that the ZGS state is mainly obtained for  $t_{c1}t_{c2} < 0$ , whereas the transfer energies ( $t_{p3}, t_{p4}, t_{c3}, t_{c4}$ ) are needed for the metallic state.

### 6. Summary and Discussion

In the present study, we examined the ZGS state by changing transfer energies within the tight-binding model. For  $-(ET)_2I_3$ , the hole and electron bands are degenerate at two contact points  $k^0$  and  $k^0$  in the first Brillouin zone. The dispersion of the electron and hole bands around the contact point resembles that of the massless Dirac Fermion, which is called the Dirac cone. In a wide pressure range (also parameters of transfer energy range), there exists the ZGS state, in which the contact point coincides with the Fermi point. The location for the contact point moves in the  $k$  space continuously when transfer energies are varied. The stability of the contact point was examined using a simplified model. The contact point moves to the symmetry axis in the Brillouin zone when the parameters are varied toward those with higher symmetry. This was also verified using the reduced model.

Let us comment on the state under the  $b$ -axis pressure  $P_b$ , which is calculated from eq. (6). When  $P_b$  is increased, the contact point still exists and moves as shown by the arrow  $P_b (< 10)$  in Fig. 5. However, the ZGS state does not appear, since the contact point is always located below the Fermi energy. The absence of the ZGS state comes from the fact that the parameters  $t_{c1}$  and  $t_{c2}$  still remain in region II of Fig. 6. In other words,  $t_{c1}$  for  $P_b$  does not increase much compared with that for  $P_a$ .

Let us examine if the ZGS state is present in other reduced models for  $-(ET)_2I_3$ . Hotta<sup>15</sup> examined a different model with two molecules in the unit cell by taking the dimer for the bond  $t_{p1}$  between 1 and 3 sites (and also that for  $t_{p2}$  between 2 and 4 sites) in Fig. 1, where the vertical transfer energies are kept. By substituting into these energies, the experimental data at ambient pressure,<sup>20</sup> the contact point below the Fermi energy is obtained at  $k^0 = (0.641; 0.694)$ . This corresponds to the metallic state, although the location of  $k^0$  differs from that of Fig. 2. For such a model, we also obtained the ZGS state under the pressure of  $P_a$ . Comparing Hotta's model with the present one, both models take into account the dimerization for the bond with the large transfer energy,

but there is a difference in the choice of the bond as seen from Fig. 1. These two kinds of pairings, which are introduced for simplicity of the calculation, seem to be almost degenerate in their energy. In the present model of  $x_5$ , the condition of  $t_{p3} = t_{p4} = t_{c3} = t_{c4} = 0$  is further introduced in order to focus on the ZGS state. There is also another reduced model for  $-(ET)_2I_3$ ,<sup>13</sup> in which  $t_{c1} = t_{c2} = t_{c3} = t_{c4}$  is taken. This model does not exhibit the ZGS state within the numerical calculation. This result may be ascribed to the fact that the ZGS state is expected mainly for  $t_{c1}t_{c2} < 0$  in Fig. 6.

Those contact points obtained in the present study are related to the "accidental degeneracy" of the bands, which was pointed out by Herring.<sup>21</sup> In the case of "accidental degeneracy", the degeneracy is not caused by the symmetry of the materials, but is caused by the intrinsic properties of the special band. As for the general case of the three-dimensional system, there appear contact lines in the Brillouin zone, which lead to a metal due to the existence of the Fermi surface. The ZGS state in  $-(ET)_2I_3$  exhibits the contact point, that always coincides with the Fermi energy, due to the quarter-filling in the highly two-dimensional system. The existence of such a degeneracy in  $-(ET)_2I_3$  has been supported recently by first-principle calculations.<sup>27,28</sup>

Anomalous properties associated with the Dirac cone have been investigated for bismuth<sup>22,23</sup> and graphite<sup>24,29</sup> using the effective Hamiltonian for the Dirac cone. In those cases the degeneracy occurs on the symmetry axis of its Brillouin zone. The effect of Berry phase due to the Dirac cone has been observed using the phase analysis of quantum oscillations.<sup>25</sup> Thus, the ZGS state of  $-(ET)_2I_3$  is also expected to exhibit many anomalous properties. The new phenomenon known as anomalous transport<sup>5,6,30</sup> may come from the Dirac cone and the unique properties of the ZGS state.

#### Acknowledgements

The authors are thankful to R. Kondo, S. Kagoshima, T. Takahashi and D. S. Hirashina for useful comments. The authors are also grateful to S. Sugawara, N. Tajima, Y. Nishio and K. Kajita for useful discussions. The present work has been financially supported by a Grant-in-Aid for Scientific Research on Priority Areas of Molecular Conductors (No.15073103) from the Ministry of Education, Culture, Sports, Science and Technology, Japan.

- 1) T. Ishiguro, K. Yamaji and G. Saito: Organic Superconductors 2nd ed. (Springer-Verlag, Berlin, 1998)
- 2) H. Seo, C. Hotta and H. Fukuyama: Chem. Rev. 104 (2004) 5005.
- 3) K. Bender, I. Hennig, D. Schweitzer, K. Dietz, H. Endres and H. J. Keller: Mol. Cryst. Liq. Cryst. 108 (1984) 359.
- 4) B. Rothaemel, L. Forro, J. R. Cooper, J. S. Schilling, M. Weger, P. Behle, H. Brunner, D. Schweitzer and H. J. Keller: Phys. Rev. B 34 (1986) 704.
- 5) K. Kajita, T. Ojiro, H. Fujii, Y. Nishio, H. Kobayashi, A. Kobayashi and R. Kato: J. Phys. Soc. Jpn. 61 (1992) 23.
- 6) N. Tajima, M. Tamura, Y. Nishio, K. Kajita and Y. Iye: J. Phys. Soc. Jpn. 69 (2000) 543.
- 7) Y. Takano, K. Hiraki, H. Miyamoto, T. Nakamura and T. Takahashi: J. Phys. Chem. Solids 62 (2001) 393.
- 8) R. Wojciechowski, K. Miyamoto, K. Yakushi, M. Inokuchi and A. Kawamoto: Phys. Rev. B 67 (2003) 224105.
- 9) T. Takahashi: Synth. Met. 133-134 (2003) 261.
- 10) M. Masato, Y. Kaga, R. Kondo and S. Kagoshima: Rev. Sci. Instrum. 71 (2000) 176.
- 11) N. Tajima, A. Ebina-Tajima, M. Tamura, Y. Nishio and K. Kajita: J. Phys. Soc. Jpn. 71 (2002) 1832.
- 12) H. Kino and H. Fukuyama: J. Phys. Soc. Jpn. 64 (1995) 4523.
- 13) H. Kino and H. Fukuyama: J. Phys. Soc. Jpn. 65 (1996) 2158.
- 14) H. Seo: J. Phys. Soc. Jpn. 69 (2000) 805.
- 15) C. Hotta: J. Phys. Soc. Jpn. 72 (2003) 840.
- 16) A. Kobayashi, S. K atayama, K. Noguchi and Y. Suzumura: J. Phys. Soc. Jpn. 73 (2004) 3135.
- 17) A. Kobayashi, S. K atayama and Y. Suzumura: J. Phys. Soc. Jpn. 74 (2005) 2897.
- 18) T. Mori, H. Mori and S. Tanaka: Bull. Chem. Soc. Jpn. 72 (1999) 179.
- 19) R. Kondo and S. Kagoshima: J. Phys. IV France 114 (2004) 523.
- 20) R. Kondo, S. Kagoshima and J. Harada: Rev. Sci. Instrum. 76 (2005) 093902.
- 21) C. Herring: Phys. Rev. 52 (1937) 365.
- 22) H. Kohno, H. Yoshioka and H. Fukuyama: J. Phys. Soc. Jpn. 61 (1992) 3462.
- 23) P. A. Wolf: J. Phys. Chem. Solids 25 (1964) 1057.
- 24) A. A. Abrikosov: Phys. Rev. B 60 (1999) 4231.
- 25) I. A. Luk'yanchuk and Y. Kopelevich: Phys. Rev. Lett. 93 (2004) 166402.
- 26) Another model for the ZGS state has also been discussed. (S. Sugawara: Master Thesis, Toho University 2005); S. Sugawara, N. Tajima, Y. Nishio and K. Kajita: private communication.
- 27) H. Kino and T. Miyazaki: J. Phys. Soc. Jpn. 75 (2006) 034704.
- 28) S. Ishibashi, T. Tamura, M. Kohyama and K. Terakura: J. Phys. Soc. Jpn. 75 (2006) 015005.
- 29) T. Ando: J. Phys. Soc. Jpn. 74 (2005) 777.
- 30) K. Kajita, N. Tajima, A. Ebina-Tajima and Y. Nishio: Synth. Met. 133-134 (2003) 95.